Earth, Planets and Space

EXPRESS LETTER

Open Access

A 3D electrical resistivity model around the focal zone of the 2017 southern Nagano Prefecture earthquake (M_{JMA} 5.6): implications for relationship between seismicity and crustal heterogeneity

Hiroshi Ichihara[1*], Junna Kanehiro[2], Toru Mogi[2], Koshun Yamaoka[1], Noriko Tada[3], Edward Alan Bertrand[4] and Mamoru Adachi[1]

Abstract

Seismic swarm areas below the southeast flank of Ontake volcano, central Japan, provide an important opportunity to study interactions between seismicity, volcanic processes and crustal fluid. On June 25, 2017, an M5.6 earthquake occurred in the Ontake swarm area where geochemical and geophysical studies suggest that pore fluid pathways from the lower crust and mantle affect fault rupture. To clarify the electrical resistivity distribution (that reflects pore fluids, altered sediments and temperature), audio-frequency and broadband magnetotelluric data were measured at 35 sites around the aftershock area of this earthquake. A 3D resistivity inversion model based on these observed magnetotelluric data shows the following key features: (1) two conductive zones (C-1 and C-2) underlie springs where isotope studies indicate fluids of mantle or lower crustal origin and (2) aftershock hypocentres locate in a resistive area between these two aseismic conductive zones (C-1 and C-2). The relationship between seismicity and conductivity suggests that the C-1 and C-2 conductors can be interpreted as interconnected pore fluid, high temperature and/or sediment under aseismic elastic conditions. In addition, the fault rupture of the M5.6 earthquake was located near the boundary between the central resistive and conductive C-2 zone, indicating stress accumulation associated with heterogeneity of rock, temperature and/or pore fluid distribution. If these features are observed generally in seismic areas, surveys of resistivity structure could contribute to estimating the magnitude of potential earthquakes and evaluation of risk.

Keywords: Crustal fluid, Earthquake swarm, Ontake volcano, Magnetotelluric, The 1984 western Nagano prefecture earthquake, Structural heterogeneity

Introduction

At Mt. Ontake volcano in central Japan (Fig. 1), previous geophysical and geochemical studies have suggested that pore fluids are associated with earthquake swarm activity located below the southeast flank of the mountain. An intra-plate earthquake (M_{JMA}5.6) occurred within the Ontake swarm area on June 25, 2017, causing significant damage. The focal mechanism of the main shock was reverse fault-type striking NNE-SSW (Nagoya University 2017), in contrast with the regional stress pattern and strike–slip mechanism (with NW–SE compression (Terakawa 2017; Yamashina and Tada 1985) of the 1984 western Nagano prefecture earthquake (M_{JMA}6.8) that occurred 5 km to the southwest. In addition, hypocenter depths of the 2017 Ontake earthquake and aftershocks

*Correspondence: h-ichi@seis.nagoya-u.ac.jp
[1] Earthquake and Volcano Research Center, Graduate School of Environmental Studies, Nagoya University, Furo-cho, Chikusa-ku, Nagoya 464-8601, Japan
Full list of author information is available at the end of the article

were significantly shallower (2–4 km from surface) (Fig. 1) compared to the surrounding earthquake swarm depths of 4–9 km (Terakawa 2017; Nagoya University 2017).

Mapping fluid pathways from the mantle to the surface is the key to understanding these anomalous shallow earthquakes and fault mechanisms. Isotope studies of spring water from the Ontake swarm area report anomalously high values of $\delta^{13}C$ from CO_2 gases, and a high $^3He/^4He$ ratio (at site SRK in Fig. 1) (Takahata et al. 2003), that indicates deep source of fluid. In addition, Li and Sr isotopic composition of spring water samples from sites SRK, KYK and KRB also indicate that crustal fluid near the 2017 earthquake area is influenced by lower crustal materials from the upper mantle (Nishio et al. 2010) (Fig. 1). These geochemical studies indicate transportation of fluid and gas from the lower crust and mantle to the surface.

While no historical eruptions have been reported, since the beginning of the earthquake swarms in 1976, Mt. Ontake volcano has repeatedly erupted in 1979, 1991, 2007 and 2014. Associated with the pyroclastic eruption in 2014, a significant increase and decrease in $^3He/^4He$ ratio of spring water samples in the earthquake swarm area was recorded before and after the eruption, respectively (Sano et al., 2015). Nishio et al. (2010) also indicated an influence of magmatic fluid to spring water in the swarm area, suggesting that crustal fluids relate to both the earthquake swarm and volcanic activities. Therefore, it is important to clarify the detailed pore fluid distribution in the earthquake swarm areas.

Previous geophysical investigations have suggested that high pore fluid content is associated with the earthquake swarm area based on *Vp/Vs* ratios from passive–seismic tomography and the subsurface resistivity distribution from MT (magnetotelluric) analysis (Doi et al. 2013; Iio et al. 2000; Kasaya and Oshiman 2004; Kasaya et al. 2002). Kimata et al. (2004) used precise-levelling measurements to detect 3–6 mm of uplift between 2002 and 2004 in an area located above the hypocenter of the 2017 earthquake. They discussed effects of mantle-derived gases to explain the crustal deformations. Terakawa et al. (2013) and Terakawa (2017) determined earthquake focal mechanisms and inferred an over-pressured fluid reservoir located beside and northeast of the aftershock area of the 2017 Southern Nagano prefecture earthquake.

While previous studies suggest that pore fluids are associated with the Ontake earthquake swarm activity, a detailed image of the pore fluid distribution in the focal area of the 2017 Southern Nagano prefecture intra-plate earthquake is required. MT observations are widely used to image subsurface electrical resistivity distribution and to detect crustal fluids since even small quantities of interconnected saline pore fluid (or melt) significantly decrease bulk rock resistivity. Previous MT studies at Mt. Ontake (Iio et al. 2000; Kasaya and Oshiman 2004; Kasaya et al. 2002) do not include measurements that cover the aftershock area of the 2017 earthquake, and utilize only 2D inversion and 3D forward modeling techniques. Here, we use a dense MT survey covering the aftershock area of the June 25, 2017, intra-plate earthquake, and use 3D inversion modeling to generate a detailed image of the electrical resistivity structure in this region. The resistivity inversion models show relationships between the subsurface distribution of fluids, crustal heterogeneity and earthquake activity in this region.

Magnetotelluric observation and Resistivity modeling

Broadband magnetotelluric (BBMT) and audio-frequency magnetotelluric (AMT) measurements were taken at 35 sites on the southeast flank of Mt. Ontake volcano between September and December 2017 (Fig. 1). These data cover the aftershock area of the M5.6 Southern Nagano Prefecture earthquake that occurred on June 25, 2017. MTU-5A and MTU-5 systems from Phoenix Geophysics Inc. were used with non-polarizing $Pb-PbCl_2$ electrodes for electric field measurement. MTC-50 induction coils for the BBMT band (0.003–1000 s) and AMTC-30 induction coils for the AMT band (0.0001–1 s) from Phoenix Geophysics Inc. were installed at all sites for magnetic field measurement. The electric and magnetic fields data were recorded for 2–5 days and 1–3 h, for BBMT and AMT measurement bands, respectively.

MT impedance estimates were computed from the observed electric and magnetic field time series data using SSMT2000 software from Phoenix Geophysics Inc. To reduce noise at each measurement site, the remote reference technique (Gamble et al. 1979) was applied for the BBMT data using horizontal magnetic field data from two permanent magnetotelluric observation stations: the Sawauchi station (located 500 km northeast of the study area) operated by Nittetsu Mining Consultants Co. and the Kubono station (located 500 km west-southwest from the study area) operated by the National Research Institute for Earth Science and Disaster Resilience (NIED). Simultaneously observed audio-frequency band magnetic field data in the study area were adapted as remote reference data for the AMT processing. At most sites, high-quality MT impedances were determined at short periods (between 0.0001 and 5 s), excluding the AMT deadband (0.0002–0.001 s) (Fig. 2). Data quality at longer periods (> 5 s) is reduced due to leakage currents associated with a DC (direct current) railway located 8–18 km east of the study area, which also affected previous MT data measured in this region (Kasaya et al.

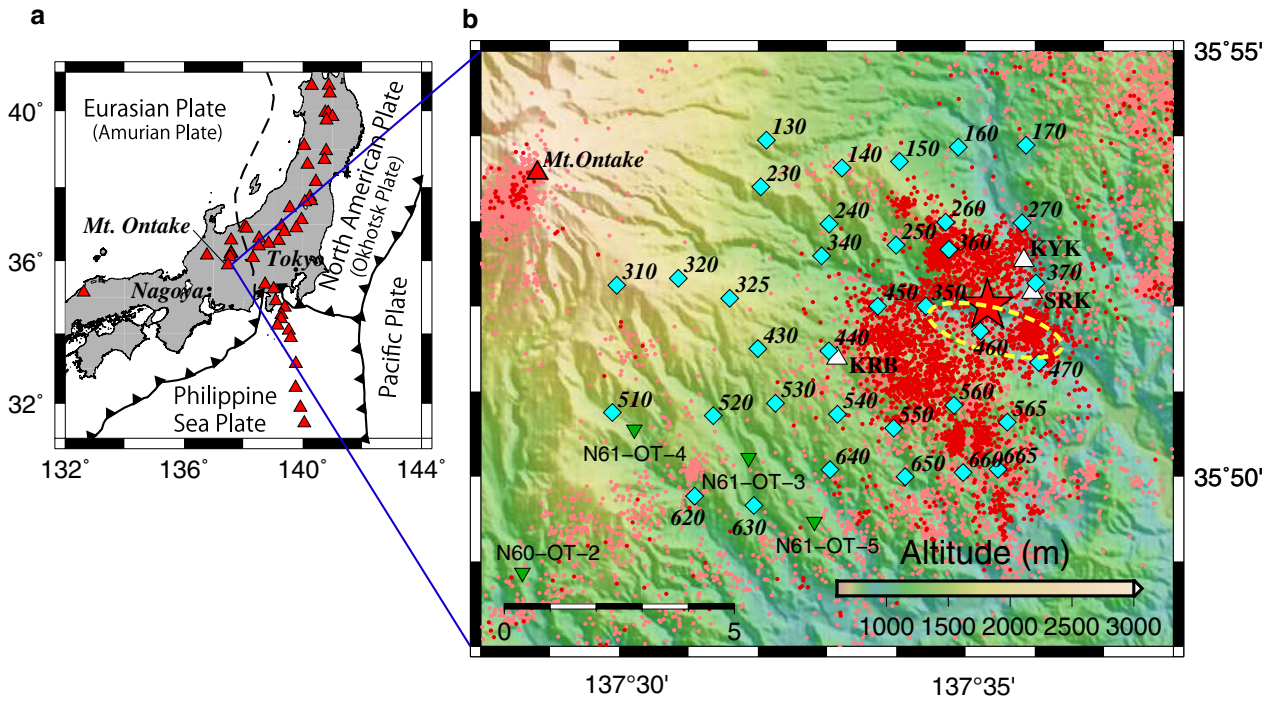

Fig. 1 **a** Index map. Red triangles denote active volcanos. Thick black lines show plate boundaries. **b** Topographic map of the study area with MT sites and seismicity. Cyan diamonds denote MT sites. Dark red and light red circles denote epicenters before and after June 24, 2017, respectively, manually estimated by Nagoya University (2017). The yellow dashed line represents the area of crustal deformation (Kimata et al. 2004). White triangles denote sampling locations of spring water indicating lower crust or mantle origin (Nishio et al. 2010)

2002). Previous studies (Kasaya et al. 2002; Kasaya and Oshiman, 2004) indicate that shallow resistivity values across the survey region are mostly over 100 Ω-m. Calculating the skin depth for a 100 Ω-m homogeneous half-space for a period of 1 s shows that our data are sensitive to Earth resistivity structure to a depth of at least 5 km.

Prior to resistivity inversion modeling, we calculate and visualize the phase tensor property, which represents the phase relationship in the measured MT impedance tensor that is free from distortion by localized heterogeneity (Caldwell et al. 2004). The phase tensor is defined as $\mathbf{\Phi} = \mathbf{X}^{-1}\,\mathbf{Y}$, where X and Y are the real and imaginary parts of the MT impedance tensor, respectively. The MT phase tensor can be graphically represented as an ellipse. A direction of the major axes of the ellipse indicates strike or its perpendicular azimuth in the 2D case. The lengths of the ellipse axes represent magnitude of the tensor principal values, $\Phi_{\max}$ and $\Phi_{\min}$, which visualize resistivity gradients. The geometric mean of the principal values ($\Phi_2 = (\Phi_{\max}\Phi_{\min})^{1/2}$) indicates the magnitude of the phase tensor response. In simple (quasi-one-dimensional) situations, decreasing resistivity with increasing depth is indicated by values of $\Phi_2 > 45°$. The skew angle β represents the tensor's asymmetry; the $|\beta|$ is large when the resistivity structure is 3D. The phase tensor ellipses (Fig. 3) show the following features. (1) A high Φ_2 area (> 50 degrees) is present in the western part of the study area at periods between 0.0013 and 0.43 s. This area shifts to the southwest at longer periods, suggesting a conductive region that dips to the south. (2) Similarly, a high Φ_2 area is observed in the northeast part at the period 0.43 and partly at periods 0.030 and 0.0013 s, also indicating the presence of a subsurface conductor. (3) Values of β are generally high ($|\beta| > 5$ degrees) and variable, indicating the three dimensionality of the resistivity structure in the study area.

A resistivity distribution in the study area is estimated with the 3D inversion code by Tada et al. (2012) which adopts a data-space variant Occam's approach. The code is based on WSINV3DMT (Siripunvaraporn et al. 2005) and is modified to treat land and marine topography. The inversion minimizes the objection function

$$W_\lambda(\mathbf{m}) = (\mathbf{m}-\mathbf{m}_p)^{\mathrm{T}}\mathrm{C}_{\mathrm{m}}^{-1}(\mathbf{m}-\mathbf{m}_p) + \lambda^{-1}\{(\mathbf{d}-\mathbf{F}[\mathbf{m}])^{\mathrm{T}}\mathbf{C}_{\mathbf{d}}(\mathbf{d}-\mathbf{F}[\mathbf{m}])\} \quad (1)$$

where $\mathbf{m}$ and $\mathbf{m}_p$ are the model and prior-model parameters, respectively. $\mathbf{C_m}$ is the model covariance matrix characterizing the expected magnitude and smoothness

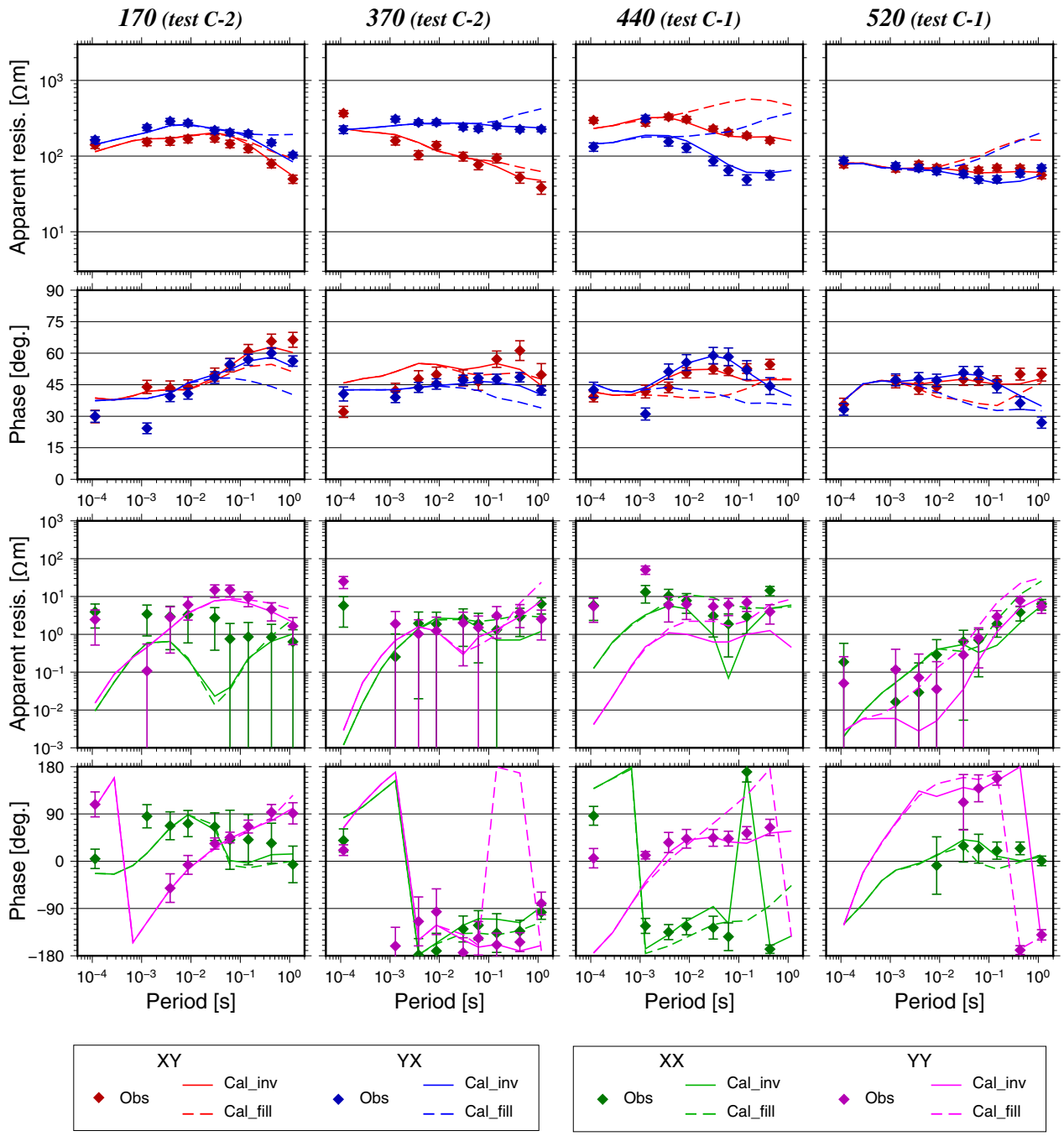

Fig. 2 Apparent resistivity and phase of MT impedances. Circles labeled "OBS" denote MT responses based on the observation. Note that the error bars include error floors for the inversion. Solid lines labeled "Cal_inv" denote model response of the inverted model. Dashed lines labeled "Cal_fill" denote the filled models. The C-2 filled model is for the sites 170 and 370, and the C-1 filled model is for sites 440 and 520. 180 degrees were added to the phases of the YX component

of resistivity variations relative to $\mathbf{m}_p$. $\mathbf{d}$ is the data parameter vector consisting of the observed MT impedances. $\mathbf{F}[\mathbf{m}]$ is the vector of the forward response to $\mathbf{m}$. λ is a hyper-parameter that balances the data misfit and model roughness terms. $\mathbf{C_d}$ is a data covariance matrix consisting of the observation errors.

We used the MT impedances at 11 periods between 0.00011 and 1.16 s as the data parameters ($\mathbf{d}$) for the

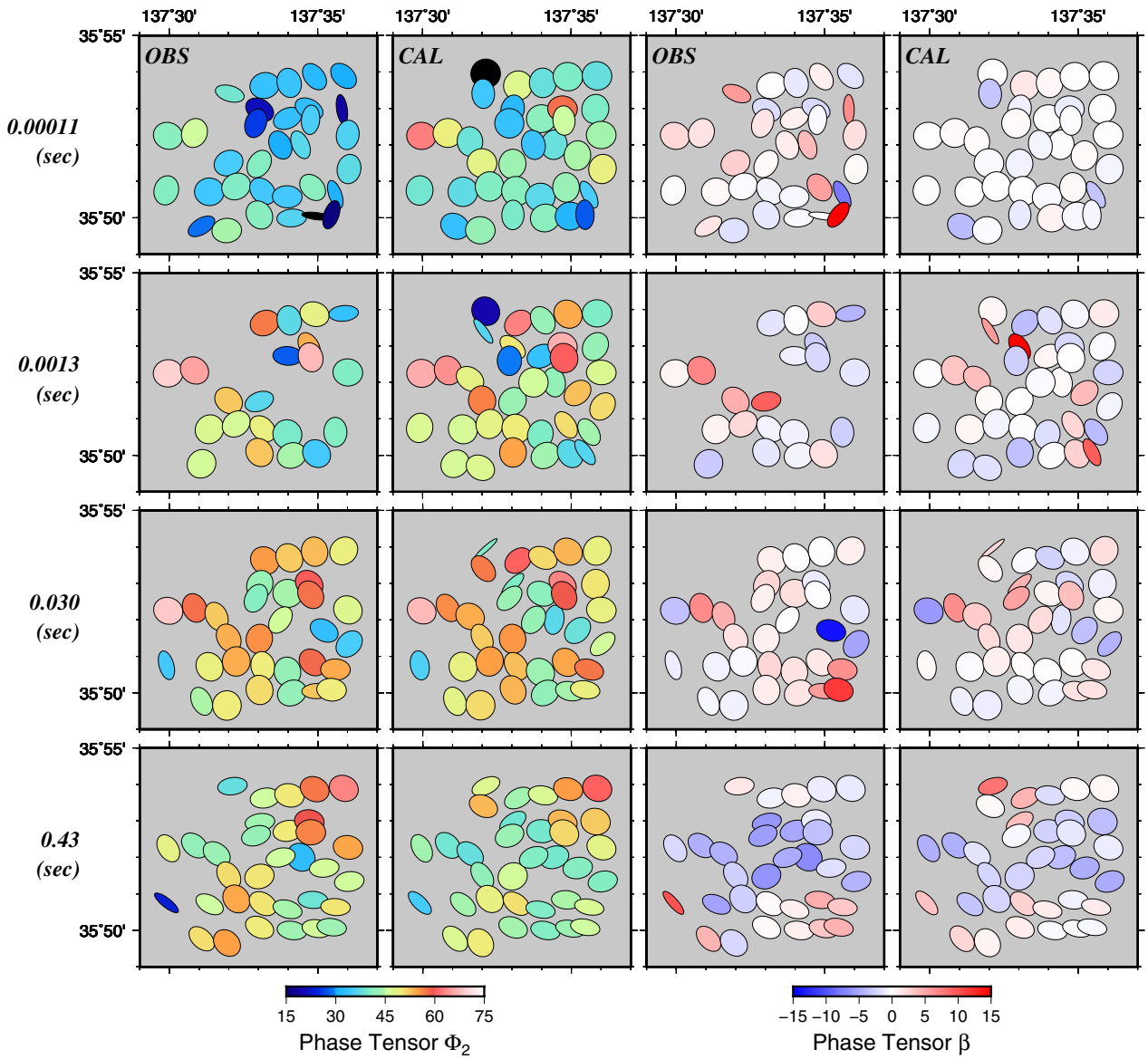

Fig. 3 Phase tensor ellipses based on observed impedance and model responses of the inverted resistivity model label as OBS and CAL, respectively

inversion with an error floor applied to all impedance components at 10% of the magnitude of the sum of the squared elements invariant (Rung-Arunwan et al. 2016; Szarka and Menvielle 1997). The total resistivity model space covered a region of 199 (x-axis) × 199 (y-axis) × 103 (z-axis, without air layers) km discretized into 43 (x-axis) × 43 (y-axis) × 120 (z-axis, including 8 air layers) blocks which is over ten times larger than the skin depth of the initial model (300 Ω-m), using the longest period included in the inversion (1.16 s). The length and width of the blocks within the survey area were 500 m, but these were widened outside the study area. The thickness of the blocks is 25 m between elevations 850 and 2175 m (relative to sea level) where the MT sites are located; block thickness below 850 m elevation is gradually increased with depth. The inversion procedure was started from an initial 300 Ω-m homogeneous model (root mean squared (RMS) misfit 6.700) and was iterated ten times. The RMS misfit was minimized in the fifth iteration (2.106) giving an acceptable fit to the observed MT impedances (Fig. 2).

The 3D resistivity inversion model shows high resistivity (> 1000 Ω-m) in the aftershock area of the 2017 earthquake,

located between two distinct low resistivity zones (C-1 and C-2) (Figs. 4 and 5). The high Φ_2 of phase tensors also imply the C-1 and C-2 conductors as we mentioned (Fig. 3). To ensure that the C-1 and C-2 conductors are robust model features, sensitivity tests were undertaken using the following procedure. First, the inversion model was modified by setting the resistivity values within the dashed line around the C-1 conductor (at depths 1–5 km; Fig. 4) to 300 Ω-m. Synthetic model responses were then computed for this "filled" model at the same locations as the field measurements, and compared to both the inverse model responses and observations (sites 440 and 452 in Fig. 2). This sensitivity test shows clearly that the filled model responses do not fit the measured data, particularly the high phase values (i.e., > 45°) and low apparent resistivity of off-diagonal components in the 0.01 s − 0.1 s period range. In addition, the RMS misfit of the filled model (3.164) was significantly increased compared to the inverted model (2.106) indicating that the C-1 conductor is required by the data and a robust model feature.

The same sensitivity procedure was undertaken to test the C-2 conductor, replacing model resistivity values with 300 Ω-m at depths 0.5–5 km within the dashed region shown in Fig. 4. Again, the filled model responses do not fit the measured resistivity and phase data (see sites 170 and 370 in Fig. 2) as well as the inverted model response, particularly at periods greater than 0.1 s. The decreased fit is also reflected in an increased RMS data misfit of 2.218, compared to 2.106. While sensitivity to the C-2 conductor is less than for C-1 (owing to the location of C-2 at depth and at the edge of the data coverage), changes in apparent resistivity and phase are significantly larger than the estimated errors. Therefore, this sensitivity test shows that the C-2 conductor is also required by the data and a robust model feature. The C-2 conductor is located at the northeastern edge of the study area and seems to extend to both the north and east. However, additional observations would be required to constrain this feature outside of our current data coverage.

Discussion

Comparison with previous resistivity models

The C-1 conductor is spatially consistent with the shallow part of a low resistivity area estimated by previous studies based on 2D resistivity inversion (Iio et al. 2000; Kasaya et al. 2002). However, these previous 2D models suggest that the low resistivity zone inclines to the north and the deeper portion partly overlaps with our C-2 conductor. In contrast, our 3D inversion model clearly images a resistive zone located between the C-1 and C-2 conductors. We infer that the resistive zone located between the C1 and C2 conductors was not detected in previous models due to: (1) the lack of MT data in the resistive area and (2) fitting measured MT responses with a smooth 2D TM-mode only inversion model. We show here an improved resistivity model with new dense MT measurements, modeled using a 3D inversion procedure.

Interpretation of the resistivity inversion model

Basement rock throughout the study area is comprised of Triassic–Jurassic accretionary complex materials of the Mino belt and intrusive granite porphyry (Takeuchi et al. 1998) (Fig. 4 and 5). These rocks are overlain in the western part of our survey by mid-late Pleistocene volcanic rocks sourced from Mt. Ontake volcano (Fig. 4). Electrical resistivity logging near the study area (inverted green triangles in Figs. 1 and 4) shows resistivity values of the Mino belt accretionary complex in the range 300–3000 Ω-m (NEDO 1988). In addition, the granites generally show very high resistivity at dry and near-surface temperature conditions. Therefore, high resistivity (> 300 Ω-m) observed throughout most of the resistivity inversion model (Fig. 4 and 5) is consistent with the expected resistivity of basement rocks in this region. In contrast, the C-1 and C-2 (10–30 Ω-m) conductors cannot be explained by typical basement rock.

Three possibilities are considered to explain the low bulk resistivity values of the C-1 and C-2 model features, (1) interconnected conductive pore fluid, (2) high temperature or partial melt and (3) conductive clay minerals such as smectite, which can be generated by alteration of the basement rock. It is plausible to consider high-temperature and/or clay-alteration mechanisms in the study area, given Pleistocene volcanic activity to the west at Mt. Ontake. However, a lack of high-temperature surface features and clay mineral occurrence reported in the surface geology and exploration geothermal boreholes (NEDO 1988) do not directly support these processes. In contrast, anomalous He and Li isotope ratios of spring water samples (Fig. 1) imply vertical transport of high-salinity (i.e., conductive) pore fluid from lower crust or mantle depths (Takahata et al. 2003; Nishio et al. 2010). In addition, areas of high *Vp/Vs* values (Doi et al. 2013) are consistent with the C-1 and C-2 conductors, and suggest a high density of water saturated cracks in these areas. Therefore, interconnected conductive pore fluid is interpreted as the most likely cause of the C-1 and C-2 model conductors. However, this interpretation does not exclude a contribution from temperature or alteration, which could also play a role in decreasing the resistivity of otherwise resistive basement rock.

Model resistivity structure could also reflect rock heterogeneity as surface geological maps show intrusive granite porphyry above the central resistive zone, and

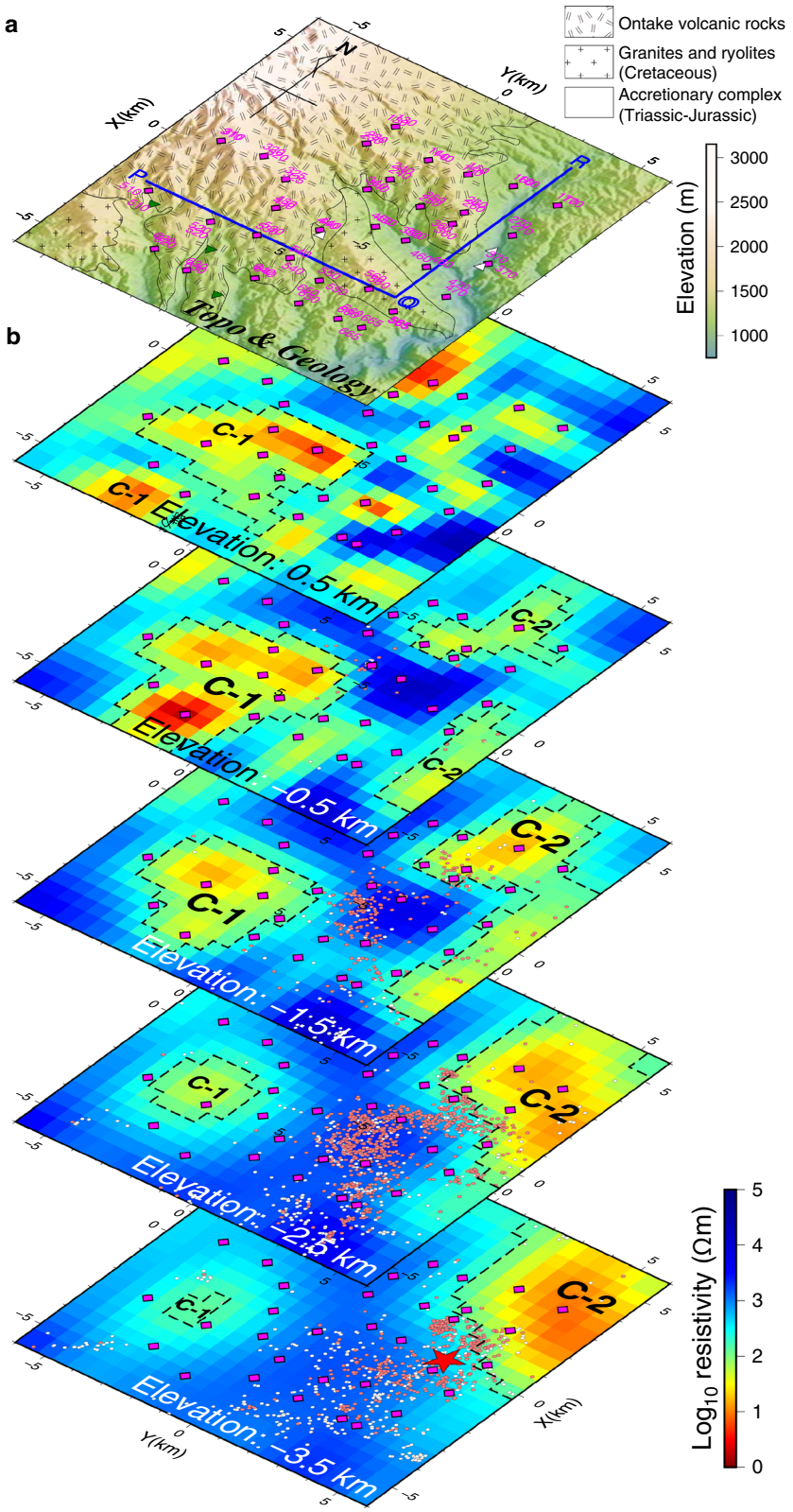

Fig. 4 **a** Topographic map with surface geology based on (Geological Survey of Japan 2015) **b** Horizontal cross section of the inverted 3D resistivity model. Magenta diamonds denote MT sites. Circles denote hypocenter locations of earthquakes that occurred between 2012 and 2017, manually estimated by Nagoya University (2017). Red and white circles indicate epicenters before and after the M_{JMA}5.6 earthquake on June 25, 2017, respectively. Area enclosed by white dashed lines shows the uniformly filled area with 300 Ω-m in the sensitivity tests. Note that only model blocks with resistivity less than 300 Ω-m are filled in the tests. Elevations are defined relative to sea level

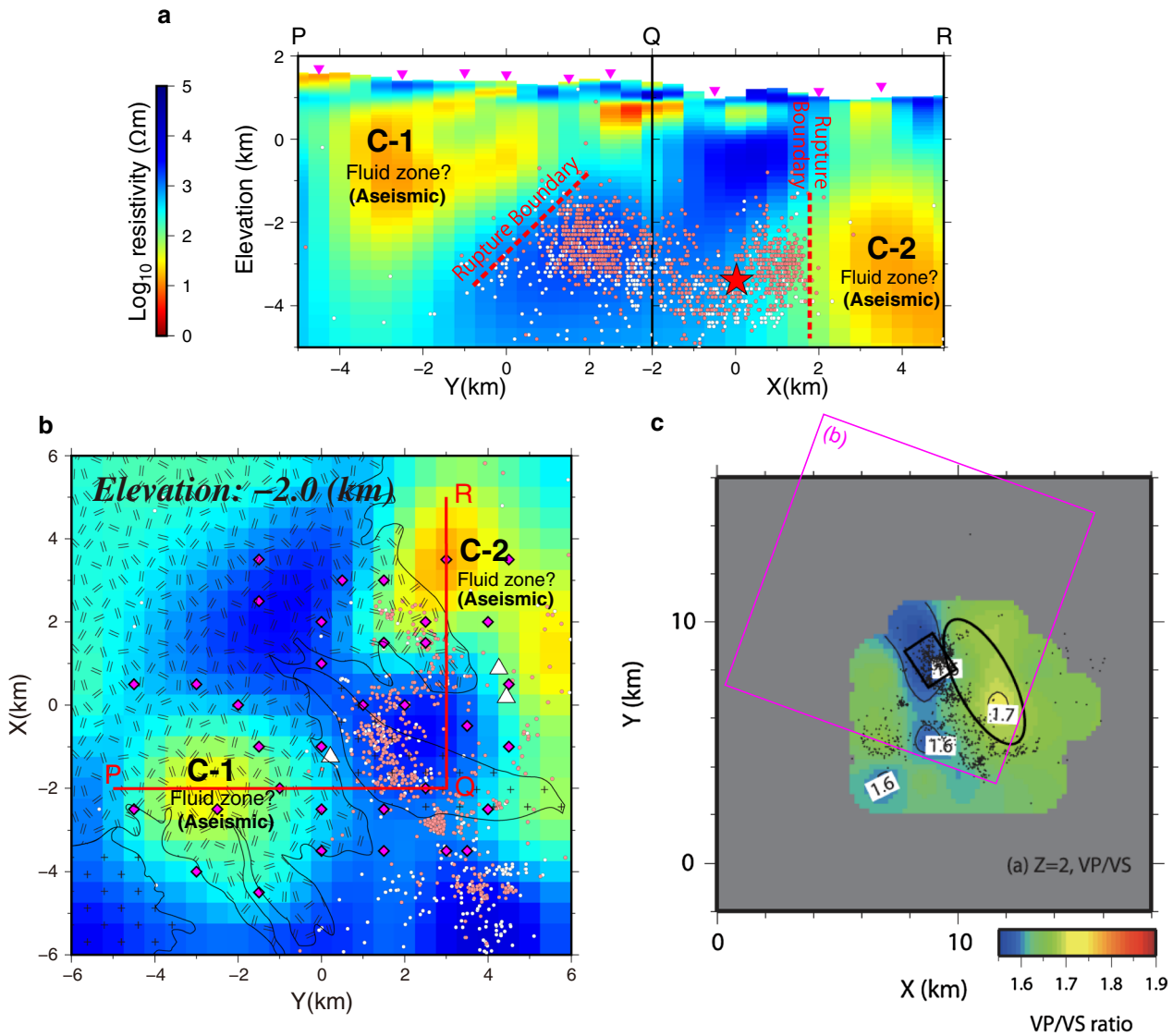

Fig. 5 **a** Vertical cross section of the 3D resistivity inversion model with interpretations along the lines P-Q and Q-R shown in Fig. 4a and 5b. Inverted triangles denote MT site locations. Other symbols are the same as in Fig. 4. **b** Horizontal cross section of the inverted 3D resistivity model (elevation − 2 km) with surface geological map. Symbols are the same as in Fig. 4. **c** Horizontal cross section of the *Vp/Vs* model by Doi et al. (2013) (elevation − 2 km). The purple rectangle shows an approximate range of (**b**)

accretionary complex materials above the C-1 and C-2 conductors. The accretionary complex in the study area (Misogawa complex in Mino belt) consists mainly of sand, stone and shale that frequently show shear deformation and are not metamorphosed (Otsuka 1988). Lower crust or mantle-derived pore fluid may therefore ascend through fractures in the accretionary complex, reducing the bulk resistivity of these rocks. This process is consistent with high *Vp/Vs* ratios observed in the C-1 and C-2 regions (Fig. 5) that suggest a high density of water saturated cracks (Doi et al. 2013). In contrast, low-permeability granites would reduce pore fluid interconnection between the C-1 and C-2 conductors, consistent with high model resistivities in this area (Fig. 5b). Similar observations were recorded in the Hidaka collision zone in northern Japan, where pore fluids derived from a plate boundary avoided areas of consolidated metamorphic rocks and ascended through an accretionary complex and/or the fractured fault zone around the boundary between the NE Japan and Kurile arcs (Ichihara et al. 2016).

Implications for seismicity

Hypocenter locations from seismicity occurring between 2012 and 2017, including aftershocks of the June 2017 Southern Nagano prefecture earthquake (M5.6), have been projected onto the resistivity model, and distribute exclusively within the central resistive part (Figs. 4, 5). The C-1 and C-2 conductive zones (interpreted as interconnected pore fluid in accretionary sedimentary rocks) are aseismic. This compelling correlation between resistivity and seismicity has been observed in other intra-plate seismic zones (Aizawa et al. 2017; Ichihara et al. 2008, 2014). Although we can only infer the elastic behavior of the C-1 and C-2 conductors by elucidation of their cause (such as pore fluid and high temperature), the correlation between conductors and aseismic areas suggests that the horizontal heterogeneity of resistivity distribution can constrain the location of seismicity. Since the 2017 southern Nagano earthquake did not propagate into the C-1 or C-2 conductors, mapping subsurface resistivity distribution may inform the maximum size of the seismogenic zone. MT data can therefore contribute to the evaluation of the potential magnitude of a fault rupture, integrated with geodetic observations and numerical studies for strain accumulations.

The distribution of the C-1 and C-2 conductors possibly indicates horizontal heterogeneity of rheology because the conductors, which were interpreted as pore fluid, high temperature and/or clay minerals, can affect rheological properties of rocks. Although earthquake occurrence is not well studied based on numerical simulations of horizontal structural heterogeneity, stress is generally accumulated outside the boundary of low-strength (ductile) regions. Locations near lateral gradients between resistive and conductive regions may therefore experience fault rupture. Previous magnetotelluric studies in other seismic areas show high seismicity near lateral resistivity gradients, which are also interpreted as horizontal elastic heterogeneity due to the presence of water or sediment (Ichihara et al. 2008; Ichihara et al. 2013; Yoshimura et al. 2009). Therefore, magnetotelluric models of subsurface resistivity can contribute to evaluating areas of stress concentration that inform earthquake risk assessment.

Conclusions

A three-dimensional resistivity inversion model of the aftershock area of the southern Nagano earthquake (M_{JMA}5.6 that occurred on June 25th 2017) based on BBMT and AMT data at 35 sites shows the following two key features: (1) Two conductive zones (C-1 and C-2) occur beneath the location of springs where isotope studies indicate fluid of mantle or lower crustal origin and (2) aftershock locations are distributed in a resistive area between the aseismic conductive zones (C-1 and C-2). The aseismic C-1 and C-2 conductive zones are interpreted as fluid-rich sedimentary rocks. These conductors bracket a high-resistivity seismogenic zone, suggesting that the resistivity distribution reflects horizontal structural heterogeneity controlling stress and strain accumulation that lead to fault rupture.

Abbreviations

MT: Magnetotelluric; AMT: Audio-frequency magnetotelluric; BBMT: Broadband magnetotelluric; NIED: National Research Institute for Earth Science and Disaster Resilience.

Authors' contributions

HI, JK, TM, KY, MA and EB contributed to magnetotelluric observations. HI, JK, NT and TM analyzed the data. All authors contributed to the interpretation and approved the final manuscript.

Author details

[1] Earthquake and Volcano Research Center, Graduate School of Environmental Studies, Nagoya University, Furo-cho, Chikusa-ku, Nagoya 464-8601, Japan. [2] Cooperative Program for Resources Engineering, Graduate School of Engineering, Hokkaido University, N13W8, Sapporo 060-8628, Japan. [3] Japan Agency for Marin-earth Science and Technology, 2-15 Natsushima-cho, Yokosuka, Japan. [4] GNS Science, 1 Fairway Drive, Avalon 5010, Lower Hutt, New Zealand.

Acknowledgements

Japan Magma Power Generation Co. financially supported this study and obtained permission for the MT observations. We also thank the landowners directly for their cooperation to establish the observation sites. The Nittetsu Mining Consultants Co., Ltd. and NIED provided us with their continuous geomagnetic records as remote references. We thank Dr. Futoshi Yamashita, NIED, for his special effort to prepare the geomagnetic data. Shin'ya Sakanaka, Graduate School of International Resource Sciences, Akita University, provided us a part of magnetotelluric instruments. Members of the earthquake and volcano research center, Graduate school of Environmental studies, Nagoya University, provided us the seismicity data and kindly joined in the discussions. We especially thank Prof. Toshiko Terakawa for these contributions. Generic Mapping Tools software (Wessel and Smith 1998) was used to draw all the figures.

Competing interests

The authors declare that there is no competing interest about this study.

Availability of data and materials

MT data used in this study are not publicly available as the field observations were supported by the Japan Magma Power Generation Co. who retain the rights to these data for commercial purposes.

Consent for publication

Not applicable.

Ethics approval and consent to participate

Not applicable.

Funding

Japan Magma Power Generation Co. supported the magnetotelluric observations.

Publisher's Note

Received: 15 August 2018 Accepted: 2 November 2018
Published online: 21 November 2018

References

Aizawa K et al (2017) Seismicity controlled by resistivity structure: the 2016 Kumamoto earthquakes, Kyushu Island, Japan. Earth Planets Space. https://doi.org/10.1186/s40623-016-0590-2

Caldwell TG, Bibby HM, Brown C (2004) The magnetotelluric phase tensor. Geophys J Int 158:457–469

Doi I, Noda S, Iio Y, Horiuchi S, Sekiguchi S (2013) Relationship between hypocentral distributions and Vp/Vs ratio structures inferred from dense seismic array data: a case study of the 1984 western Nagano Prefecture earthquake, central Japan. Geophys J Int 195:1323-1336. https://doi.org/10.1093/gji/ggt312

Gamble TD, Clarke J, Goubau WM (1979) Magnetotellurics with a remote magnetic reference. Geophysics 44:53–68

Geological Survey of Japan (2015) Seamless digital geological map of Japan 1: 200,000. May 29, 2015 version

Ichihara H, Honda R, Mogi T, Hase H, Kamiyama H, Yamaya Y, Ogawa Y (2008) Resistivity structure around the focal area of the 2004 Rumoi-Nanbu earthquake (M 6.1), northern Hokkaido, Japan. Earth Planets Space 60:883–888. https://doi.org/10.1186/BF03352841

Ichihara H, Mogi T, Yamaya Y (2013) Three-dimensional resistivity modelling of a seismogenic area in an oblique subduction zone in the western Kurile arc: constraints from anomalous magnetotelluric phases. Tectonophysics 603:114–122. https://doi.org/10.1016/J.Tecto.2013.05.020

Ichihara H et al (2014) A 3-D electrical resistivity model beneath the focal zone of the 2008 Iwate-Miyagi Nairiku earthquake (M 7.2). Earth Planets Space. https://doi.org/10.1186/1880-5981-66-50

Ichihara H, Mogi T, Tanimoto K, Yamaya Y, Hashimoto T, Uyeshima M, Ogawa Y (2016) Crustal structure and fluid distribution beneath the southern part of the Hidaka collision zone revealed by 3-D electrical resistivity modeling. Geochem Geophy Geosy 17:1480–1491. https://doi.org/10.1002/2015gc006222

Iio Y, Ikeda R, Omura K, Matsuda Y, Shiokawa Y, Takeda M, Uehara D (2000) Conductivity structure of seismogenic region in the western Nagano prefecture. Butsuri-Tansa 53:56–66 **(in Japanese with English abstract)**

Kasaya T, Oshiman N (2004) Lateral inhomogeneity deduced from 3-D magnetotelluric modeling around the hypocentral area of the 1984 western Nagano Prefecture earthquake, central Japan. Earth Planets Space 56:547–552. https://doi.org/10.1186/BF03352514

Kasaya T, Oshiman N, Sumitomo N, Uyeshima M, Iio Y, Uehara D (2002) Resistivity structure around the hypocentral area of the Western Nagano Prefecture earthquake in central Japan. Earth Planets Space 54:107–118. https://doi.org/10.1186/BF03351711

Kimata F et al (2004) Ground uplift detected by precise leveling in the Ontake earthquake swarm area, central Japan in 2002-2004. Earth Planets Space 56:E45–E48. https://doi.org/10.1186/BF03353324

Nagoya University (2017) Southern Nagano prefecture earthquake on June 25, 2017. http://wwwevrc.seis.nagoya-u.ac.jp/ontake/201706EV/

NEDO (1988) Report on promoting geothermal development, vol 17 (Otaki area) **(in Japanese)**

Nishio Y, Okamura K, Tanimizu M, Ishikawa T, Sano Y (2010) Lithium and strontium isotopic systematics of waters around Ontake volcano, Japan: implications for deep-seated fluids and earthquake swarms. Earth Planet Sci Lett 297:567–576. https://doi.org/10.1016/j.epsl.2010.07.008

Otsuka T (1988) Paleozoic-Mesozoic sedimentary complex in the eastern Mino terrane, central Japan and its Jurassic tectonism. J Geosci Osaka City Univ 31:63–122

Rung-Arunwan T, Siripunvaraporn W, Utada H (2016) On the Berdichevsky average. Phys Earth Planet In 253:1–4. https://doi.org/10.1016/j.pepi.2016.01.006

Sano Y, Kagoshima T, Takahata N, Nishio Y, Roulleau E, Pinti DL, Fischer TP (2015) Ten-year helium anomaly prior to the 2014 Mt Ontake eruption. Sci Rep-Uk. https://doi.org/10.1038/srep13069

Siripunvaraporn W, Egbert G, Lenbury Y, Uyeshima M (2005) Three-dimensional magnetotelluric inversion: data-space method. Phys Earth Planet In 150:3–14

Szarka L, Menvielle M (1997) Analysis of rotational invariants of the magnetotelluric impedance tensor. Geophys J Int 129:133–142. https://doi.org/10.1111/j.1365-246X.1997.tb00942.x

Tada N, Baba K, Siripunvaraporn W, Uyeshima M, Utada H (2012) Approximate treatment of seafloor topographic effects in three-dimensional marine magnetotelluric inversion. Earth Planets Space 64:1005–1021. https://doi.org/10.5047/Eps.2012.04.005

Takahata N, Yokochi R, Nishio Y, Sano Y (2003) Volatile element isotope systematics at Ontake volcano, Japan. Geochem J 37:299–310. https://doi.org/10.2343/geochemj.37.299

Takeuchi M, Nakano S, Harayama S, Otsuka T (1998) Geology of the Kiso-Fukushima district with geological sheet map at 1:50,000. Geological Survey of Japan, p 94 **(in Japanese with English abstract 4p)**

Terakawa T (2017) Overpressurized fluids drive microseismic swarm activity around Mt. Ontake volcano, Japan. Earth Planets Space. https://doi.org/10.1186/s40623-017-0671-x

Terakawa T, Yamanaka Y, Nakamichi H, Watanabe T, Yamazaki F, Horikawa S, Okuda T (2013) Effects of pore fluid pressure and tectonic stress on diverse seismic activities around the Mt, Ontake volcano, central Japan. Tectonophysics 608:138–148. https://doi.org/10.1016/j.tecto.2013.10.005

Wessel P, Smith WHF (1998) New, improved version of generic mapping tools released. EOS Trans Am Geophys U 79(47):579

Yamashina K, Tada T (1985) A fault model of the Western Nagano prefecture earthquake based on distance change of trilateration points. Bull Earthq Res Inst 60:221–230

Yoshimura R et al (2009) Magnetotelluric transect across the Niigata-Kobe Tectonic Zone, central Japan: a clear correlation between strain accumulation and resistivity structure. Geophys Res Lett. https://doi.org/10.1029/2009gl040016